11-26-2015

Collisional Excitation of [C II], [O I] and CO in Massive Galaxies

R. E. A. Canning
Stanford University

Gary J. Ferland
University of Kentucky, gary@uky.edu

A. C. Fabian
University of Cambridge, UK

R. M. Johnstone
University of Cambridge, UK

P. A. M. van Hoof
Royal Observatory of Belgium, Belgium

See next page for additional authors

Monthly Notices of the ROYAL ASTRONOMICAL SOCIETY

MNRAS **455,** 3042–3057 (2016) doi:10.1093/mnras/stv2390

Collisional excitation of [C II], [O I] and CO in massive galaxies

R. E. A. Canning,[1,2]★ G. J. Ferland,[3,4] A. C. Fabian,[5] R. M. Johnstone,[5] P. A. M. van Hoof,[6] R. L. Porter,[7] N. Werner[1,2] and R. J. R. Williams[8]

[1]*Kavli Institute for Particle Astrophysics and Cosmology (KIPAC), Stanford University, 452 Lomita Mall, Stanford, CA 94305-4085, USA*
[2]*Department of Physics, Stanford University, 452 Lomita Mall, Stanford, CA 94305-4085, USA*
[3]*Department of Physics and Astronomy, University of Kentucky, Lexington, KY 40506, USA*
[4]*Centre for Theoretical Atomic, Molecular and Optical Physics, School of Mathematics and Physics, Queens University Belfast, Belfast BT7 1NN, UK*
[5]*Institute of Astronomy, Madingley Road, Cambridge CB3 0HA, UK*
[6]*Royal Observatory of Belgium, Ringlaan 3, 1180 Brussels, Belgium*
[7]*Stellar Science Ltd Co. 6565 Americas Parkway NE, Suite 925, Albuquerque, NM 87110, USA*
[8]*AWE plc, Aldermaston, Reading RG7 4PR, UK*

Accepted 2015 October 14. Received 2015 October 13; in original form 2014 December 9

ABSTRACT

Many massive galaxies at the centres of relaxed galaxy clusters and groups have vast reservoirs of warm (∼10 000 K) and cold ($\lesssim$100 K) gas. In many such low-redshift systems this gas is lifted into the hot interstellar medium in filamentary structures, which are long lived and are typically not forming stars. Two important questions are how far do these reservoirs cool and if cold gas is abundant what is the cause of the low star formation efficiency? Heating and excitation of the filaments from collisions and mixing of hot particles in the surrounding X-ray gas describes well the optical and near infrared line ratios observed in the filaments. In this paper we examine the theoretical properties of dense, cold clouds emitting in the far infrared and sub-millimetre through the bright lines of [C II] λ157 μm , [O I] λ63 μm and CO, exposed to such energetic ionizing particles. We find that optical depth effects and thermal pressure support alone cannot account for the line ratios; however, a very modest additional pressure support can fit the observed [O I] λ63 μm/[C II] λ157 μm line ratios by decreasing the density of the gas. This may also help stabilize the filaments against collapse leading to the low rates of star formation. We make predictions for the line ratios expected from cold gas under these conditions and present diagnostic diagrams for comparison with further observations. We provide our code as an Appendix.

Key words: ISM: clouds – galaxies: clusters: general – galaxies: clusters: intracluster medium – intergalactic medium – submillimetre: ISM.

1 INTRODUCTION

The Herschel telescope opened up a wealth of lines in the far infrared (FIR) such as the strong fine structure cooling lines of [O I] λ63 μm and [C II] λ157 μm . These emission lines, which are often attributed to the presence of photo-dissociation regions (PDRs), excited by far Ultra-Violet (FUV) emission from young stars (e.g. Hollenbach & Tielens 1999), have been found in a number of brightest cluster galaxies (BCGs; e.g. Edge et al. 2010a,b; Mittal et al. 2011, 2012; Werner et al. 2013) and in X-ray and radio bright giant elliptical (gE) galaxies (Guillard et al. 2015; Werner et al. 2014). In these dense, X-ray bright systems the cooling time of the hot gas is short; an important consequence of which is that a heat source is required to prevent catastrophic cooling of the intracluster medium (ICM) which would lead to unprecedented growth of the galaxy. This heating is likely provided by active galactic nucleus (AGN) feedback (for a review see Fabian 2012).

Though sample sizes are small, where extended ionized emission lines have been observed, Herschel observations of [C II] λ157 μm have shown the cold ($T \lesssim 100$ K) gas is also extended and coincident with the ionized filaments (Werner et al. 2013, 2014). Werner et al. (2014) also show that the Hα/[C II] λ157 μm ratio is similar, implying that the ionized and cold gas share a common excitation mechanism. Though evidence for some star formation is observed in BCGs (e.g. Hubble & Humason 1931; Johnstone, Fabian & Nulsen 1987; McNamara & O'Connell 1989; Allen 1995; Crawford et al. 1999; McNamara, Wise & Murray 2004; Hicks & Mushotzky 2005; McNamara et al. 2006; O'Dea et al. 2008, 2010; Quillen et al. 2008; Rafferty, McNamara & Nulsen 2008; Canning

★ E-mail: rcanning@stanford.edu

et al. 2010; Donahue et al. 2010; Hicks, Mushotzky & Donahue 2010; McDonald et al. 2012), many of these extended filaments have no obvious star formation despite the large quantities of cool and cold gas. PDRs are therefore an unlikely heating mechanism.

The ionized filaments are thought to be long-lived but their energy source and the reason for their quiescence have been a puzzle. H_2, CO, dust and polycyclic aromatic hydrocarbon (PAH) features have been shown to exist coincident with some ionized filaments (e.g. Jaffe & Bremer 1997; Falcke et al. 1998; Donahue et al. 2000, 2011; Edge 2001; Jaffe, Bremer & van der Werf 2001; Edge et al. 2002; Wilman et al. 2002; Salomé & Combes 2003; Crawford et al. 2005; Hatch et al. 2005; Jaffe, Bremer & Baker 2005; Salomé et al. 2006, 2011; Johnstone et al. 2007; Wilman, Edge & Swinbank 2009; Oonk et al. 2010; Canning et al. 2013). The new information garnered from the low-ionization and molecular emission lines seen by Herschel and the high spatial resolution made available by Atacama Large Millimeter/submillimeter Array (ALMA) will be instrumental in probing density and temperature-sensitive lines with which to characterize the properties of the cold gas, and in allowing the morphology and kinematics of this gas to be mapped on the same spatial scales as the optically emitting ionized filaments (e.g. McNamara et al. 2014; Russell et al. 2014).

The dichotomy between the lack of gas observed in central galaxies in galaxy clusters and groups without dense, cool X-ray cores and its abundance in many cool-core clusters indicates that cooling from the X-ray gas must be important in these systems (e.g. Cavagnolo et al. 2008). However, why these extended gas reservoirs continue to shine has been an issue of contention; optical emission-line ratios are typically 'LINER-like' (low ionization nuclear emission-line region; however it is important to note that these are not 'nuclear' regions). However, it has been shown that many physical processes can produce similar LINER-like ratios (weak shocks; e.g. Sparks, Macchetto & Golombek 1989; Farage, McGregor & Dopita 2012; hot stars e.g. Terlevich & Melnick 1985; conduction e.g. Voit & Donahue 1997; Sparks et al. 2012, mixing with hot gas which leads to both collisional excitation and thermal excitation of the gas e.g. F2009; Fabian et al. 2011 and dissipation from magnetic reconnection in magnetically supported filaments e.g. Churazov, Ruszkowski & Schekochihin 2013).

Ferland et al. (2008, 2009) (hereafter F2009) have suggested collisions with the surrounding energetic particles as a mechanism for heating the multi-phase filaments. The authors show that their model, which allows the filaments to be described by cloudlets of varying densities, can successfully reproduce the ratios of the near infrared (NIR) strong H_2, and optical atomic and low ionization emission lines, which has been a struggle for photoionization models. The model also reproduces the characteristic signatures of relatively high He I and [N I] emission and of relatively low [O III] in the extended filaments (Johnstone & Fabian 1988; Voit & Donahue 1997; Sabra, Shields & Filippenko 2000; Hatch et al. 2005; Canning et al. 2011), while allowing anomalously high [Ne III] emission, through charge-transfer reactions. However, the models are unable to match recent Herschel observations of the ratios of [O I] λ63 μm and [C II] λ157 μm in the filaments. It should be noted that the authors stress their model is applicable only to optically thin clouds and additionally that the data used in F2009 cannot constrain a large reservoir of cold clouds in the filaments as the power law controlling the composition of the cloudlets is hinged on emission lines from gas at 10^4–1000 K.

Collisional excitations and ionizations of atomic and molecular gas by high-energy particles are probably important, not only in the filaments of BCGs, but also in a wide range of astrophysical environments such as the opaque molecular cores of PDRs where heating is thought to be dominated by excitations produced by cosmic rays (e.g. Hollenbach & Tielens 1997), in cool and cold gas near AGNs (e.g. Shull & van Steenberg 1985) and also in the cool gas filaments expelled in the death throes of supernovae where non-thermal electrons are generated by the hard synchrotron photoionizing source (e.g. Richardson et al. 2013).

The best, nearby, example of an extended ionized and molecular web surrounding a BCG is NGC 1275. Some regions of this extended web are forming stars but the majority are not (Conselice, Gallagher & Wyse 2001; Canning et al. 2010, 2014). Obviously, where cool gas is close to intense photoionization from stars, such as in the inner regions of some BCGs or in star-forming filaments, this photoionization will contribute significantly to the excitation of the gas. We must therefore look at 'clean' regions, devoid of obvious star formation in order to examine the excitation mechanism for the filaments prior to their degeneration into stars, or evaporation into the hot ISM/ICM. *Hubble Space Telescope* (*HST*) SBC data show that the star formation rate in a 'typical' non-star-forming region, of NGC1275's filaments, assuming all the UV flux is due to stars, is <0.001 $M_\odot$ yr^{-1}(Johnstone et al. 2012).

The two questions of basic importance are how much cold gas exists and if cold gas is abundant what is the cause of the low rate of star formation? Focusing on these questions we investigate the effect of energetic particles on the cold gas $\lesssim$100 K in the filaments. We have extended the models of F2009 to explore the physical and chemical states of the cold ($T \lesssim 100$ K) gas with densities ranging from $n = 10^0$ to 10^6 cm^{-3}, and in particular we consider the effects of finite column densities of individual cloudlets. Our primary aim is to explore the discrepancy between the observed and predicted line ratios of the FIR fine structure lines of [O I] λ63 μm and [C II] λ157 μm in the extended filaments of BCGs. However, our models are generally applicable to ionized, neutral and molecular gas exposed to energetic ionizing particles. The spectrum from collisional heating in cool and cold gas clouds is complicated as it depends sensitively on changes in the heating and cooling of the gas which in turn depends on much of the physics of the cloud.

Section 2 reviews briefly the details of the particle heating model grid and discusses the physical and chemical properties of the grid. Section 3.1 explores the effect of a large quantity of cold clouds on the composite model spectrum for BCGs. Section 3.2 discusses the effects of optical depth on the predictions for the BCG line ratios and Sections 3.3 and 3.4 explore the effect of turbulence and magnetic fields. Some words of caution about the models are given in Section 3.5. A discussion and predictions for future observations are presented in Section 4.

2 MODEL

The particle heating model used in this paper is essentially that described in F2009 for optically thin emission from warm ionized gas adapted to include physics pertinent to very cold clouds. The model is motivated by spectra from extended emission-line regions in BCGs which show spatially coincident emission from molecular, atomic and ionized gas, suggesting that the total emission in the filaments is from clouds with a range of densities and temperatures. F2009 parametrize the contribution of the different phases to the total volume as a weighted sum of 'cloudlets' of different densities but constant pressure. The weighting function, α, is taken to be a power law in the cloud density, and hence the cloud density function

will be this power law. The line emissivity ($4\pi\bar{j}$ in erg cm^{-3} s^{-1}) summed over the distribution of clouds is

$$4\pi\bar{j} \simeq \sum_{i=0}^{k} 4\pi j_i(n_i) n_i^{\alpha-1} \Delta n_i / \sum_{i=0}^{k} n_i^{\alpha-1} \Delta n_i, \quad (1)$$

where n_i are the specific densities and we simulate the grid in density bins of 0.1 dex from $\log_{10}(n)$ 0 to 6.

The pressure in the ionized filaments has been measured by Heckman et al. (1989) and is similar to the X-ray derived pressure of the ICM. Throughout the paper we will refer to 'hot gas' as X-ray emitting ($T \gtrsim 10^6$ K) gas, 'warm gas' as ionized, optical emitting clouds ($T \sim$10 000 K) which emit strongly in Hα, 'cool gas' as $T \sim 1000$ K gas which emits strongly in H_2 12 μm and 'cold gas' as gas with temperatures $T \lesssim 100$ K, which emit in the strong fine structure lines of [C II] λ157 μm , and many molecular emission lines.

F2009 use the Hα and H_2 12 μm emission-line ratios to determine α for the Perseus cluster (a constant pressure of $\sim 10^{6.5}$ cm^{-3} K is used for the Perseus cluster). They find $\alpha = -0.35$ can reproduce all emission lines from the warm ionized ($T \sim$ 10 000 K) gas to within a factor of 2 (but see Johnstone et al. 2012 for a discussion of the Hα flux in the Perseus cluster). This value of α implies the majority of the volume is filled by hot ionized gas with only a minor contribution from the more massive, cold clouds. Hα emission is predominantly from $\sim 10^4$ K gas while the H_2 12 μm emission line is from gas $\sim 10^3$ K. The authors point out that the data available at the time are not able to constrain a large reservoir of very low temperature clouds. However, extrapolation of α to low-temperature clouds gives good agreement with mass estimates from CO emission lines though these may be optically thick (Salomé et al. 2011). Extrapolating this model of optically thin lines to the very cold $\lesssim$100 K gas, the simple model predicts [O I] λ63 μm/[C II] λ157 μm ratios of ∼20. However, the observed line ratios are $\leqq$1 (Mittal et al. 2011, 2012; Werner et al. 2013, 2014). A myriad of physical processes could be responsible for this discrepancy in the observed ratio.

The calculations in this paper were made using Cloudy C13 (Ferland et al. 2013) and we provide our code in Appendix A. As in F2009, due to the longevity of the filaments, we neglect regions in which the cooling is thermally unstable. We caution here that this may not be the case in the cold filaments and the line ratios in some lines are sensitive to this assumption (see Section 2.1). Chatzikos et al. (2015) studied the effects of non-equilibrium cooling but found it not to be important in the hot gas (>10^4 K).

The models shown here are of a cloud where the farthest edge from us is not open, that is photons cannot escape out the far side of the cloud. While un-physical we choose to show these models due to simplicity of explaining the underlying physics of the emission lines. We have repeated all our calculations with an open-ended cloud; the only difference in results occurs in the last zone where the temperature of the open ended cloud drops as photons can escape. This drop in temperature has the effect of slightly decreasing the emissivity in the emission lines which remain optically thin such as Hα. No significant effect is observed in the integrated line ratios. The largest physical size of the last zone in any calculation is <100th of the final depth of the cloud, typically the size of the last zone is <1000th of the final depth.

Cloudy contains a grain model which resolves the size distribution of the grains and can calculate the grain properties, such as the charge distribution, temperature and grain opacities separately for grains of a given radius. The grain photoelectric heating can then be determined for graphite, silicate and PAH features separately. A description of the Cloudy grain model is given in van Hoof et al. (2001, 2004). We include dust grains with an ISM abundance and PAHs using the distribution from Bakes & Tielens (1994) with an abundance of $10^{-4.6}$ carbon atoms per hydrogen atom in PAH features. The Jura rate is assumed for the formation of H_2 on grains and the dissociation of H_2 is calculated self-consistently within Cloudy. The Jura rate is used to ensure our results are directly comparable with F2009; however, we additionally test points in the grid using H_2 formation rates from Cazaux & Tielens (2002) which depend on grain temperature and abundance. Grain temperatures in the dense regions are <40 K and most emission-line emissivities vary by <5 per cent with Hα emission varying by <15 per cent. [O I] λ63 μm/[C II] λ157 μm line ratios vary by <5 per cent using H_2 formation rates from Cazaux & Tielens (2002).

In F2009 simulations are of a representative unit volume of gas. The actual filament is envisioned as being composed of many such parcels with a range of densities, temperatures, and ionizations and also with a range of column densities. For this approach to work the simulation of the unit volume is set to be optically thick in all resonance lines, as would happen if part of a much larger column density. Cloudy calculates a full model of the hydrogen atom and its emission physics. We use this model in the predictions in this paper but assume that the Lyman lines are all optically thick. The effect of this optical depth is to stop fluorescent pumping by the metagalactic background, and prevent Lyman lines produced in the recombination process from freely escaping. Rather, Lyman lines undergo a large number of scatterings and are converted into Balmer and other lines, are absorbed by dust, or escape from the cloud.

The variable parameters in the particle heating model are the density of ionizing particles measured relative to the Galactic cosmic ray background and the volume density of hydrogen in the gas, n. The energy density of the Galactic cosmic ray background is $\sim$1.8 eV cm^{-3} which corresponds to a pressure of ionizing particles of $\sim 2 \times 10^4$ K cm^{-3}. In the centre of the Perseus cluster, Sanders & Fabian (2007) find an electron energy density ∼1000 times the Galactic background. We investigate the effect of ionizing energetic particles over a range of values corresponding to ∼1 to $\sim 10^7$ times the density of the Galactic cosmic ray background and gas densities of ∼1 to $\sim 10^6$ hydrogen nuclei per cm cubed.

2.1 Integration limits

As mentioned in the previous section, the calculations in this paper neglect regions in which the cooling is thermally unstable. Thermal stability for a constant pressure gas is given by

$$\left[\frac{\partial(C-H)}{\partial T}\right]_P = \left[\frac{\partial(C-H)}{\partial T}\right]_\rho - \frac{\rho_0}{T_0}\left[\frac{\partial(C-H)}{\partial \rho}\right]_T > 0, \quad (2)$$

where C is the cooling rate, H is the heating rate, P is the pressure, ρ is the density and T is the temperature (Field 1965; see also fig. 13 of F2009). Fig. 1 shows the emissivity versus temperature profiles of Hα and many lines from cold gas for the zero turbulence case. The bottom panel shows the cooling multiplied by the temperature. The thermally unstable regions of the grid are shown by the shaded regions and the line emissivity in these regions, or equivalently cloudlets with these temperatures, are not included in the integral. The significance of the emission from thermally unstable regions to the total emissivity in the line will depend on the cloud density distribution, α. For most strong emission lines the thermally unstable regions do not make a significant contribution to the overall emission. However, for Hα the emissivity in the thermally unstable region at high temperatures ($10^4 - 10^5$ K) is ∼5 per cent of the total for $\alpha = 0$.

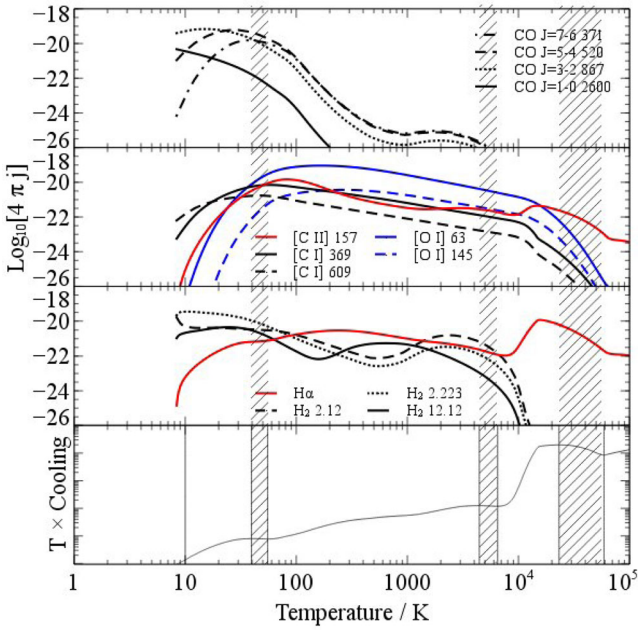

Figure 1. The temperature dependence of the emissivity of some FIR and sub-mm cooling lines. The regions where the gas is thermally unstable are shaded. These are determined by from the cooling$\times T$ curve in the bottom panel.

We choose a temperature of 10^5 K, as our upper integration limit, when integrating the emissivities from the cloud distribution. The emission from cool and cold gas has very little emissivity beyond a few 10^4 K so the choice of upper limit of the integral has negligible effect on the total emission in the lines. However, this may not be the case for the low-temperature integration limits. The lowest temperature point in the grid, at each density, occurs where there is no additional ionizing particle flux. At this point the excitation in the gas is only by the background cosmic ray ionization radiation (we assume a mean H^0 ionization rate of 2×10^{-16}s^{-1} from Indriolo et al. 2007.), the CMB, and the ISM photoionizing radiation field. We caution that the total emission from some lines from very cold gas, such as low J lines of CO, is sensitive to this lower limit cut-off.

2.2 Overview of physical and chemical properties of the grid

Ionized and cold gas filaments in BCGs are situated in the hot ISM, surrounded by the X-ray emitting galaxy halo. The penetrating nature of X-rays means they can input energy locally into cold and dense clouds creating partially ionized regions within predominantly atomic or molecular gas. The X-ray photons action is to: one, ionize; two, excite; or three, heat the gas. The contribution of each of these mechanisms depends on both the ionization fraction ($X_e = n_e/n$) of the gas and its composition, whether the gas is mostly atomic or molecular. It is less sensitive to the shape of the ionizing continuum, and the absolute values of the electron (n_e) or hydrogen (n) densities. Additionally, electrons and ions with a high kinetic temperature exist in the hot halo which can also penetrate the filaments and ionize and excite the cold gas. In this paper we model the effects of the energetic secondary electrons which will arise in the cold clouds from these processes.

In neutral gas most of the ionization and excitation by the supra-thermal electrons will be of H^0 due to both its larger abundance and larger cross-sections for interaction compared with other neutral elements or first ions. Ionization and excitation of He^0 and He^+ will be the next most important interactions. Primary and Auger ionization will lead to secondary electrons which can collisionally ionize or excite other species in the gas. Excitation will generate line photons which both can interact further with the gas or may escape the cloud causing the gas to cool. Finally, direct heating of the gas is achieved through Coulomb collisions (see Maloney, Hollenbach & Tielens 1996 for an in-depth description of X-ray irradiation of cold dense clouds).

The temperature, total pressure and ionization fraction of the gas are shown in Fig. 2 for the simple, optically thin particle heating model; no additional pressure from turbulent motions or magnetic fields are included. In all three plots the thick black contour indicates a gas pressure of $\sim 10^{6.5}$ cm^{-3} K, appropriate to the Perseus cluster of galaxies. As expected, as we increase the flux of ionizing particles, for fixed density, the temperature, pressure and ionization fraction increase. For a fixed flux of ionizing particles, increasing the density of the cloudlet corresponds to a decrease in the temperature and an increase in the pressure. As the temperature decreases so does the ionization fraction.

Where the ionization fraction ($X_e = n_e/n$) is greater than a few per cent, Coulomb collisions with the thermal electron population dominate the interactions of the supra-thermal electrons and provide the majority of the heating in the cloud (see Fig. 2). When X_e falls below 1 per cent ionizations of neutral hydrogen dominate with excitations also becoming increasingly important (Shull & van Steenberg 1985; Maloney et al. 1996). The ionization structure of hydrogen, oxygen and carbon, for a range of ionizing particle densities and hydrogen densities, is shown in Fig. 3. H^0 persists over much of the parameter space with the gas becoming fully ionized at several tens of thousands of kelvin and fully molecular at only a few tens. In atomic gas, when the energy of the electrons drops below the smallest excitation energy, all of the remaining energy must go into heating the gas. Therefore, for a gas dominated by neutral hydrogen, once the supra-thermal electron energy falls below 10.2 eV, Coulomb heating is the only heating process. So a low ionization fraction in atomic gas leads to a low heating efficiency (Shull & van Steenberg 1985; Xu & McCray 1991).

At high densities and low temperatures the gas transitions to a primarily molecular phase, where collisions with H_2 dominate, though pockets of ionized and atomic regions will remain. Heating is more efficient in molecular gas and is dominated by collisional de-excitation of vibrationally excited H_2 molecules and by H_2 dissociation by photons and ionization by secondary electrons. Significant amounts of energy can also go into the excitation of the rotation–vibration bands of H_2 and into the dissociative electronic states (Glassgold & Langer 1973; Voit 1991). In Fig. 2 the temperature increases around a density of $10^{3.3}$ cm^{-3}. This is due to the increase in the H_2 gas fraction leading to a higher heating efficiency.

Fig. 4 shows the variation in the emissivity of the Hα, [O I] λ63 μm and [C II] λ157 μm emission lines, respectively, across the whole parameter space. The dashed line in each case indicates the excitation temperature of the line from the ground while the dotted black lines indicates the critical densities (for collisions with electrons) of the lines; $n_{cr}^{[OI]} = 5 \times 10^5$ cm^{-3} and $n_{cr}^{[CII]} = 3 \times 10^3$ cm^{-3}. However, it should be noted that electrons are not the only colliders in the gas.

Collisional excitation is the dominant contributor to the line emission in all regions of the plot. Above the excitation temperature, collisions are dominated by both thermal electrons and secondary electrons; below this temperature the emissivity is dominated by

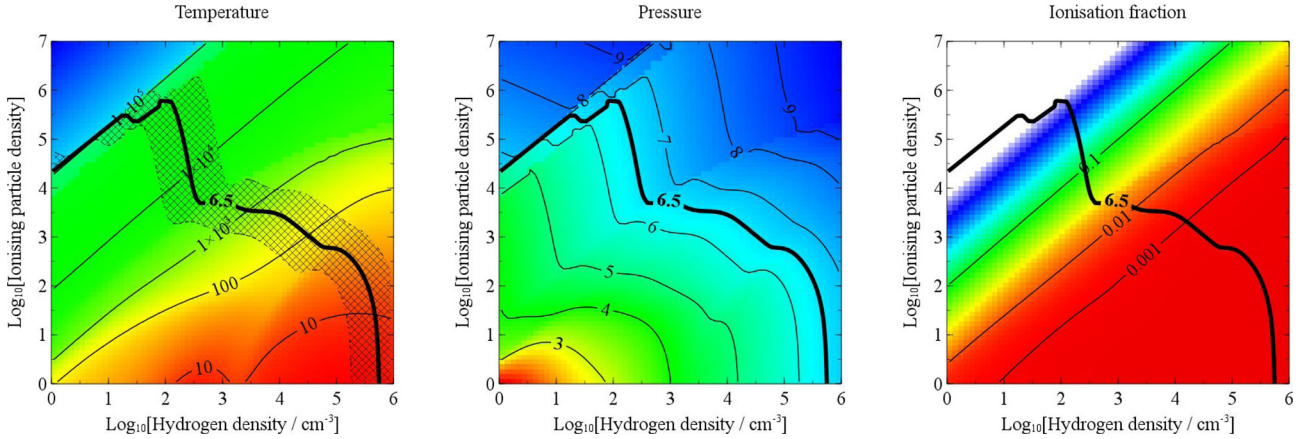

Figure 2. Left: the temperature of the cloud. For the optically thin case the temperature on this plot is the temperature of each 'cloudlet' and in the optically thick case it will be the surface temperature of the cloud. The solid black line represents a total pressure of $10^{6.5}$ cm^{-3} K (the gas pressure, derived from X-ray measurements, of the core of the Perseus cluster) and the hatched area represents pressures from 10^{6} to 10^{7} cm^{-3} K. Middle: contours of the total gas pressure in the simple optically thin, non-turbulent case with no additional pressure from magnetic fields. Right: ionization fraction, X_e (electron density, n_e, divided by particle density, n), of the gas for the same model.

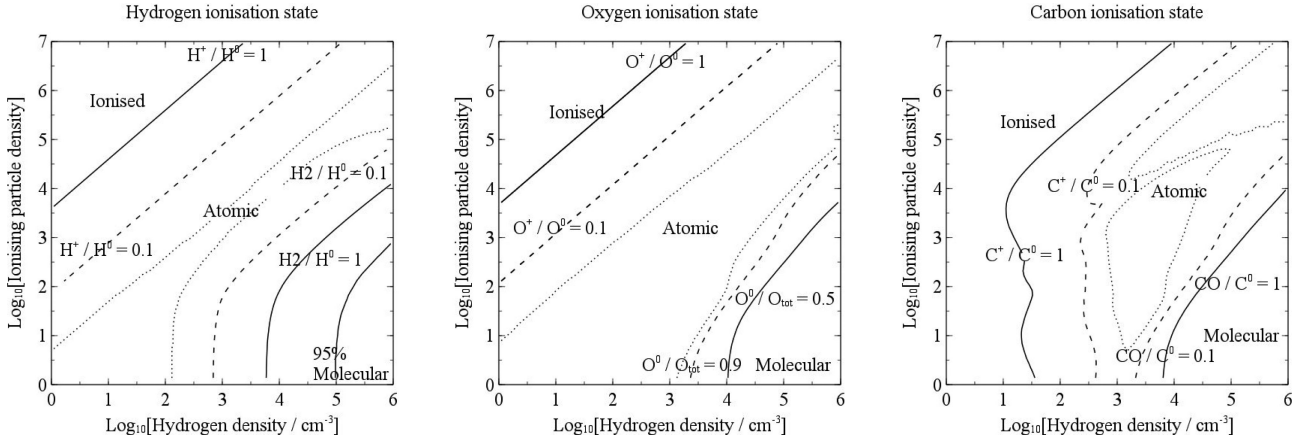

Figure 3. The ionization structure of hydrogen, oxygen and carbon. The solid contours indicate where the atomic species and the ionized/molecular species have the same abundance. The dashed contours indicate where the gas is 90 per cent atomic and the dotted contours show where the gas is 98 per cent atomic.

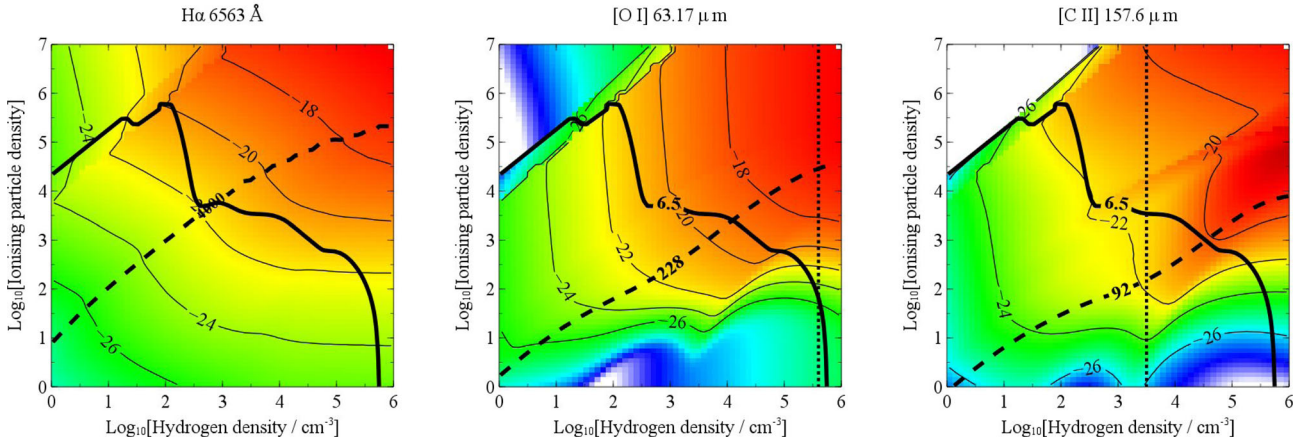

Figure 4. The log emissivity of the Hα (left), [O I] λ63 μm (middle) and [C II] λ157 μm (right) emission lines for the simple model. The contour of constant gas pressure, relevant to the Perseus cluster ($10^{6.5}$ cm^{-3} K), is drawn as a solid black line on each plot. The dashed black lines indicate the excitation temperature of the line from ground while the dotted black lines indicate the critical density of the emission line. In the optically thin model we integrate the emissivity of each line for a given pressure over a weighted density distribution.

collisions with secondary electrons and atomic hydrogen. In the coldest, densest regions of the grid collisions with H_2 dominate. In our model Hα emission in the filaments arises from collisions with both thermal and secondary electrons (see upper panel of fig. 15 of F2009), and the geometry of the resulting clouds will be permeated by pockets of high and low temperature in a 'Swiss-cheese-like' fashion. The degree of polarization expected from the model is therefore complex (see also Sparks et al. 2014).

The emissivity of the collisionally excited lines is essentially proportional to $n_a n_b f(T)$ where n_a and n_b are the species colliding and $f(T)$ is the Boltzmann factor of the line for the case where collisions are occurring with thermal particles and is a constant for the case where the collisions are occurring with supra-thermal secondary electrons. Therefore, moving towards the lower right hand corner of Fig. 4, where the temperature is too low for collisional excitation by thermal particles, at constant density the emissivity will increase by a more-or-less constant amount which is proportional to the number of secondary electrons available to collide with. The approximate flattening of the emissivity for constant ionizing particle density with increasing hydrogen density is due to the high abundance of targets, such as H^0 and H_2, compared with the low abundance of ionizing secondaries; increasing the density does not affect the emissivity much as the collision rate coefficients for collisions with H^0 and H_2 are smaller. The supra-thermal particles prevent the gas from becoming fully molecular even in the densest regions.

As the temperature of the gas increases and we move towards the upper left hand side of the plot collisions by thermal particles also become important and the line emissivity is less sensitive to the number of ionizing particles. Significantly above the excitation temperature the emissivity remains essentially constant with increased gas temperature until the temperature is high enough that most atoms are ionized and the line emissivity drops.

3 COMPLICATING THE MODEL

3.1 Additional cold clouds

The formalism presented in F2009 describes the cloud in terms of a weighted sum of very small 'cloudlets' of different density phases but at constant pressure. The weighting function is parametrized as a fraction of the total volume filled by each phase and an assumption is made that the function takes the form of a power law in density. The total emissivity is found by integrating the density-dependent emissivity over the cloud distribution (see equation 1).

In reality, we do not know the shape of the cloud distribution which may be highly complex; in practice, a power law is chosen for simplicity. Physically, the variation of the power-law index (α) tells us the contribution to the total emissivity in a particular emission line, from gas of different temperatures, thus a relatively high α would show regions where dense, cold gas dominates over warmer less dense regions. As the cloud is assumed to maintain a constant gas pressure a simple relation exists for the temperature and total particle density.

The left hand plot of Fig. 5 shows the ratio of [O I] λ63 μm over [C II] λ157 μm predicted for a grid of ionizing particle fluxes and cloud densities. The hashed region shows where contours of constant pressure of 10^6 cm^{-3} K to 10^7 cm^{-3} K lie. If a power law is not an appropriate parametrization for the coldest clouds then their predicted ratios will be different. For example, at a pressure of $10^{6.5}$ cm^{-3} K in gas with a temperature of $T < 25$ K ($n > 10^{5.1}$) [C II] λ157 μm dominates over [O I] λ63 μm emission while at higher temperatures the contrary is true.

Assuming that the power law is not an appropriate parametrization for the coldest gaseous phases the most efficient way to produce a low ratio of [O I] λ63 μm over [C II] λ157 μm would be by adding additional cold clouds where the ratio is very low. Fig. 1 shows for a constant pressure cloud with $10^{6.5}$ cm^{-3} K, the [O I] λ63 μm over [C II] λ157 μm ratio is lowest ($\sim$0.05) for hydrogen densities of $\sim 10^{5.6}$ cm^{-3} and where the ionizing particle density is of the order of $10^{1.5}$ times the Galactic cosmic ray background.

The cloud density distribution will thus be described by a power law with index α and an additional delta function where the ratio of [O I] λ63 μm over [C II] λ157 μm is lowest. We require the emissivity of these additional cold clouds to be a factor of 1.8×10^4 times that expected for an ensemble of clouds with the same properties, in order for the [O I] λ63 μm over [C II] λ157 μm ratio to be $\sim$1. However, the addition of more cold clouds has a significant effect on the other line ratios. Importantly, Hα and H_2 12.28 μm are significantly stronger for high-density, low-temperature clouds than [C II] λ157 μm by factors of $\sim$100 and $\sim$20 000 times, respectively, which is not observed in the filaments (see Fig. 5).

3.2 Optically thick lines

The majority of the lines of interest in F2009 are optically thin, thus validating the use of a unit volume of gas in the predictions of the line ratios. However, as previously mentioned, some lines in the wavelength range of Herschel and ALMA may become optically thick at reasonable column densities and as such require special attention.

The intensity of radiation from a cloud decreases along its path due to scattering and absorption and increases due to spontaneous and stimulated emission. For an optically thin plasma, all radiation generated within the plasma is able to leave it, spontaneous emission is all that is required and the matter is not in thermal equilibrium with the radiation. Hence, an optically thin source will radiate below the blackbody limit. In an optically thick system photons are absorbed and re-emitted many times before leaving the cloud and the cloud is considered to be at a quasi-equilibrium temperature where emission from the cloud in all directions will be the same. This sets an upper limit to the intensity obtained at a specific frequency from a thermal source at a specific temperature and is the blackbody limit. The luminosity in the line, per steradian, at the blackbody limit can be estimated by

$$L_{\rm line} = T_{\rm b} f_{\rm v} \Delta V \pi R^2 = \left(\frac{h\nu}{k_{\rm B}}\right) \frac{1}{{\rm e}^{\frac{h\nu}{k_{\rm B}T}} - 1} f_{\rm v} \Delta V \pi R^2 \qquad (3)$$

where ΔV is the velocity width of the line in km s^{-1}, due to micro turbulence, $f_{\rm v}$ is the velocity filling factor, and $T_{\rm b}$ is the line's brightness temperature in K. For [O I] λ63 μm and [C II] λ157 μm we cannot make the simplifying assumption that $h\nu \ll kT$.

Mittal et al. (2011) have observed [C II] λ157 μm and [O I] λ63 μm line emission using Herschel, in NGC 1275, and measure line widths of a few hundred km s^{-1}. The flux expected at the blackbody limit is therefore $\sim 1 \times 10^{-16}$ W m^{-2} for [C II] and $\sim 6 \times 10^{-15}$ W m^{-2} for [O I] (with a filling factor of 1). The measured flux of [C II] λ157 μm is comparable to that of the blackbody limit while the measured flux of [O I] λ63 μm is a factor of 100 lower.

This is a very conservative limit as the real velocity width of the line is likely to be a lot smaller. Salomé et al. (2008a) measure line widths of the CO $J = 2$–1 line in NGC 1275 in the Perseus cluster with the 2.5 arcsec beam of the Plateau de Bure Interferometer, to

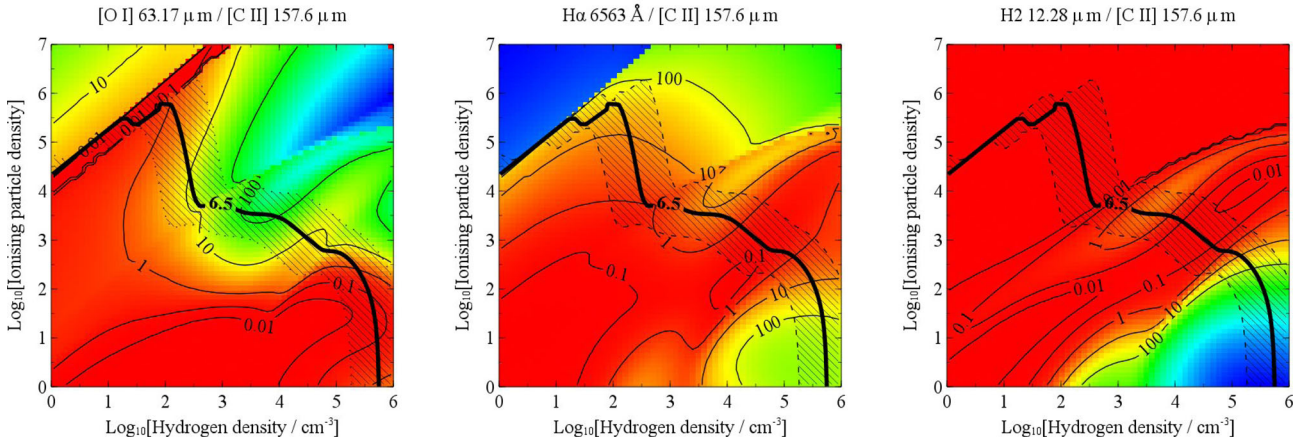

Figure 5. Left: the line ratio, [O I] λ63 μm/[C II] λ157 μm , calculated for an optically thin cloud for different hydrogen densities and ionizing particle densities. The ratio is very sensitive to variations in the cloud properties. The contour of constant total pressure, relevant to the Perseus cluster ($10^{6.5}$ cm^{-3} K), is drawn as a solid black line. The ratio increases towards the top right-hand corner of the grid. This corresponds to an increase in density at constant temperature and can be understood as the critical densities of the [O I] lines are much larger than that of the [C II] lines. The middle and right plots respectively show the ratio of the emissivity of Hα to that of [C II] λ157 μm and the ratio of the emissivity of H_2 12.28 μm to that of [C II] λ157 μm for the same optically thin clouds. Observationally Hα/[C II] λ157 μm ∼1.3 (Mittal et al. 2012; Werner et al. 2014) and H_2 12 μm/[C II] λ157 μm ∼0.025 (F2009).

be as low as ∼30 km s^{-1} . The smallest Herschel angular resolution is 5 arcsec, while the cool ionized gas filaments are determined, with the *HST*, to have an upper limit of only 0.2 arcsec (70 pc) wide in Perseus. It is therefore very likely, within this large aperture, that the velocity width is dominated by the macro turbulence of many intertwined filaments, not the micro turbulence of the emission line.

To explore the effect of high column density on the predictions of the particle heating model we will first make the simplifying assumption that the cloud is at one initial temperature and model the emergent line intensities of important IR cooling lines for clouds of different column density. In this manner we are studying conditions across a finite column density cloud with surface properties corresponding to a single point in Fig. 2. We show in Fig. 6 the emission-line ratios of [O I] λ63 μm/[C II] λ157 μm and [O I] λ63 μm/[O I] λ145 μm for four such models with surface temperatures of 15 K, 33 K, 60 K, and 100 K at a pressure of ∼$10^{6.5}$ cm^{-3} K ; the emissivity profiles of many cold gas lines are shown in Fig. B1.

Fig. 6 shows that for a constant pressure cloud, even at low initial temperature, [O I] λ63 μm/[C II] λ157 μm >1 once the lines are optically thick. This is expected from the blackbody limit, assuming the emission lines come from the same gas, given in equation (3). If both lines are saturated we expect [O I] λ63 μm/[C II] λ157 μm ∼3, therefore under equilibrium conditions and assuming no additional pressure support in the gas, an optically thick gas is not sufficient to explain the observed line ratios of [O I] λ63 μm and [C II] λ157 μm in the filaments.

The [O I] λ63 μm and [O I] λ145 μm emission lines should be produced from the same clouds so this ratio has less degeneracies than the [O I] λ63 μm/[C II] λ157 μm ratio and can be a more sensitive test of the optical depth in the lines. In the optically thick limit, for a reasonable range of temperatures, Fig. 6 shows that the ratio of [O I] λ63 μm/[C II] λ157 μm should be lower than that which has currently been observed (observations are indicated by the grey region.). We note that in many cases [O I] λ145 μm is too weak to be detected and as such the upper limit to the grey region is likely to increase with deeper observations. In addition, in the no-turbulence case for lines with temperature $\lesssim$100 K the [O I]63 μm line becomes optically thick around a column density of ∼10^{22} cm^{-2}, corresponding to a high extinction of $A_V = 5.6$ (assuming $N_H = 1.8 \times 10^{21} A_V$ from Predehl & Schmitt 1995) The [C II] λ157 μm and [O I] λ145 μm lines become optically thick at columns which are prohibitively large (see also Liseau, Justtanont & Tielens 2006).

3.3 Turbulence

In the previous sections, and in the F2009 model, no turbulence was included in the lines. We currently only have upper limits on the turbulent motions of a single cloud in the extended filaments of BCGs as the beam size is large compared with the filament threads. Optical and NIR observations of the filaments typically measure line widths, of gas at ∼1000 and 10 000 K, to be between 50 and 200 km s^{-1} (Lim et al. 2012) while Salomé et al. (2008a) have measured line widths of ∼30 km s^{-1} , in the cold gas, using the 2.5 arcsec beam of the Plateau de Bure Interferometer in the extended filaments of NGC 1275. The 2.5 arcsec beam is ∼12 times the upper limits on filament thread width determined by the *HST* (Fabian et al. 2008). All these observations currently suffer from confusion of filament threads.

In Galactic giant molecular clouds line widths are typically measured as a couple of km s^{-1} in the molecular gas with measurements of a few km s^{-1} in the cold and warm neutral mediums (Hennebelle & Chabrier 2013). Under 100 K, the sound speed is already less than 2 km s^{-1} while in <30 K gas the sound speed is below 1 km s^{-1} so molecular clouds may be turbulent in the molecular and possibly cold neutral phases. Kritsuk & Norman (2011) show that scaling relations found between the ^{12}CO(J = 1–0) line-width and size and mass and size of molecular clouds (Larson 1981) can be interpreted as a signature of supersonic motion. Other supporting evidence for supersonic motions come from the measurement of a log normal distribution of the column density (Vazquez-Semadeni 1994). However, while turbulence predicts a log normal distribution it is not necessary that a log normal distribution implies turbulence (Tassis et al. 2010).

Micro-turbulence increases the line width which suppresses the optical depths and alters the importance of shielding and pumping of lines. Self-shielding becomes less important while the ability to

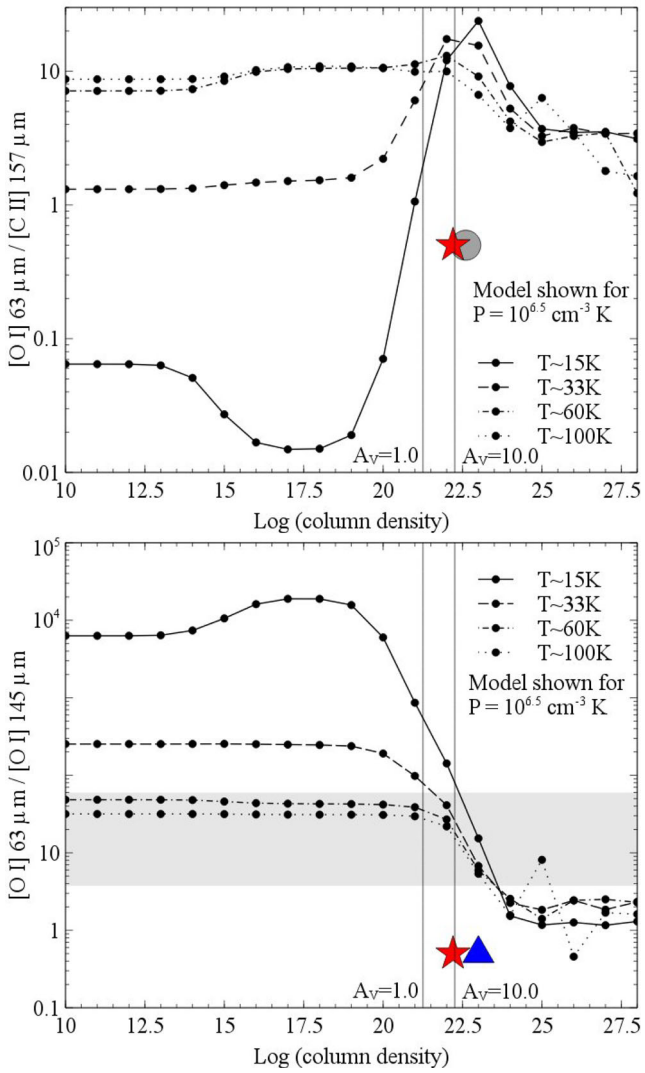

Figure 6. The predicted [O I] λ63 μm/[C II] λ157 μm (top) and [O I] λ63 μm/[O I] λ145 μm (bottom) line ratios versus column density for cloudlets at a constant pressure of $\sim 10^{6.5}$ cm^{-3} K, but with varying surface temperatures (no turbulence or magnetic fields are included in the models shown). The red star, grey circle and blue triangle indicate the peak in emission of [O I] λ63 μm, [C II] λ157 μm and [O I] λ145 μm, respectively, for a cloud with surface temperature 33 K. The location of the peak emission varies only marginally with initial conditions over the surface temperatures shown (see Fig. B1). At high optical depths the [O I] λ63 μm/[C II] λ157 μm ratio tends to a few, this is larger than is observed. Observational [O I] λ63 μm/[C II] λ157 μm ratios in the filaments are typically less, <1. In the bottom plot, the grey region shows the currently detected values for the [O I] λ63 μm/[O I] λ145 μm line ratio; we note that in many cases the [O I] λ145 μm emission line is too weak to detect. These line ratios favour optically thin gas at 'warm' temperatures (50–100 K).

absorb a larger part of the continuum increases the importance of florescence. Our initial grids, of the emissivities of the emission lines, shown in Fig. 4 are not affected by the addition of turbulence as in this simple model all lines are assumed optically thin. We note here our cloudy models do not include shock heating of the gas.

As well as altering the chemical balance, the introduction of microturbulence affects the pressure balance of the cloud. Cloudy includes the turbulence as a velocity in km s^{-1}, $u_{\rm turb}$. The additional energy density is therefore $P_{\rm turb} = \frac{F}{6}\rho u_{\rm turb}^2$, where ρ is the gas density and F is a constant which accounts for how ordered the turbulent velocity field is. We assume $F = 3$, appropriate for isotropic turbulent motions but note that the filaments are likely threaded with magnetic fields which would influence the turbulent motions of ions (Heiles & Crutcher 2005).

The effect of the additional pressure term significantly alters the predicted line ratios, from cold gas, for reasonable values of $u_{\rm turb}$. The gas pressure contour required to keep the filament in pressure equilibrium with the surrounding hot gas is reduced as shown in Fig. 7. Essentially, when the turbulent pressure is large the gas cools at constant density. The turbulent pressure is density dependent and as such the largest deviation from the no-turbulence curve, for a constant turbulent velocity at all temperatures, is in the densest gas phases. As can be seen in Fig. 7 this will alter the ratios of [O I] λ63 μm/[C II] λ157 μm , pushing them to lower ratios while leaving those of higher temperature lines unchanged.

Turbulent dissipation would also lead to heating of the gas. We can estimate the contribution of the turbulent heating to the gas line luminosity using

$$L_{\rm turb} = \frac{3M_{\rm tot}v_{\rm turb}^3}{2l}{\rm ergs}^{-1}, \quad (4)$$

where $M_{\rm tot}$ is the gas mass, $v_{\rm turb}$ is the turbulent velocity and l is the injection scale of the turbulence. We assume the very conservative values of $M_{\rm tot} \sim 10^6 {\rm M}_\odot$ and $v_{\rm turb} \sim 10\,{\rm km\,s}^{-1}$. The scale is the largest unknown, not least because individual filament threads have not been resolved, and so we assume here $l \sim 1/4$ *HST* filament width limit ~17 pc. These values lead to $L_{\rm turb} \sim 5.5 \times 10^{37}$ erg s^{-1}. In the horseshoe filament chosen as a typically example filament by F2009 in NGC 1275, the authors find an Hα luminosity of 7 $\times 10^{39}$ erg s^{-1}. The [C II] λ157 μm /Hα ratio is ~0.8 so $L_{\rm [CII]} \sim 5.6 \times 10^{39}$ erg s^{-1}. The turbulent heating is therefore only one per cent of the line luminosity. A turbulent velocity of ~45 km s^{-1} is required to reach the [C II] λ157 μm line luminosity, or alternatively $l \sim 0.17$ pc. However, this still neglects the luminosity of H_2, CO and other important lines.

3.4 Magnetic fields

The presence of strong magnetic fields in the filaments of BCGs has been inferred from optical observations of the geometry and widths of single threads of extended filaments (Fabian et al. 2008), from radio observations (Taylor et al. 2006) and implied from density arguments (Werner et al. 2013). However, magnetic fields have never been directly detected in the filaments. If these strong fields exist they will increase the energy density, $P_{\rm mag} = \frac{B^2}{8\pi}$, also decreasing the contribution to the total pressure budget from gas pressure.

In our implementation B is a constant and not dependent on density. This may not be the case but a full treatment is beyond the scope of the paper. As the B field is not density dependent, the additional pressure is a constant in all cloudlets and as such the required gas pressure is less at all densities. This is shown graphically by the contours in Fig. 8. Importantly, as in the case of additional turbulent support, the required density of the coldest gas is less dense than in the fiducial model which decreases the predicted ratios of [O I] λ63 μm over [C II] λ157 μm . However, this implementation will affect all line ratios; the optical and IR lines from the 10 000 K−1000 K gas as well as the FIR and sub-mm lines from much colder gas.

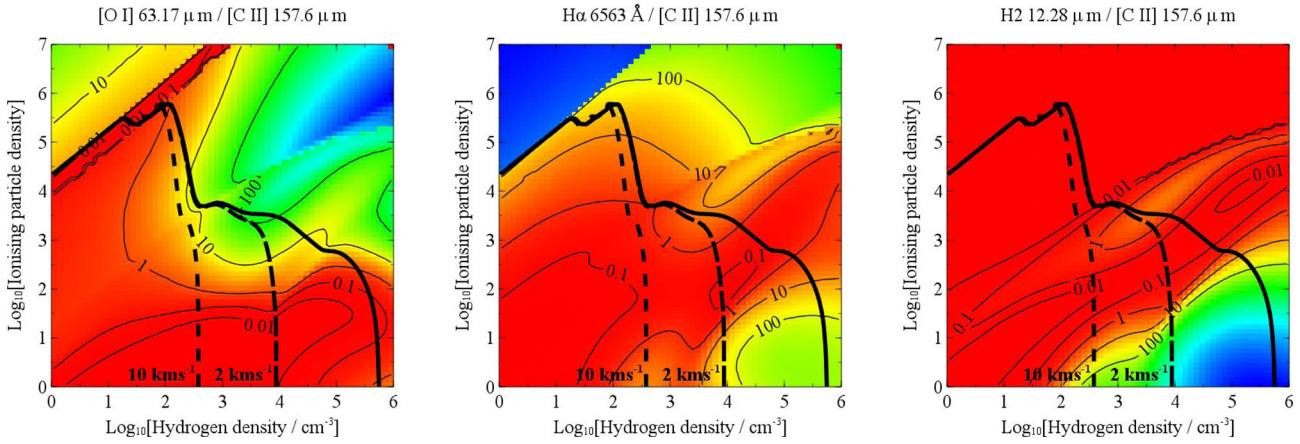

Figure 7. The ratios of key lines overlaid with contours of gas pressure in the cases where none, 2 $\mathrm{km\,s^{-1}}$ and 10 $\mathrm{km\,s^{-1}}$ turbulence is present in the gas. The grids were recalculated under these conditions but the variations in the shown line ratios are negligible so we plot them here on one grid. Left: [O I] λ63 μm/[C II] λ157 μm . Middle: Hα / [C II] λ157 μm . Right: H_2 12.28 μm/[C II] λ157 μm . The measured fluxes are the integral of the cloudlets, indicated by the pressure contour. Observationally, the fluxes are [O I] λ63 μm/[C II] λ157 μm $\lesssim 1$, Hα/[C II] λ157 μm ∼1.3 (Mittal et al. 2012; Werner et al. 2014) and H_2 12 μm/[C II] λ157 μm ∼0.025 (F2009).

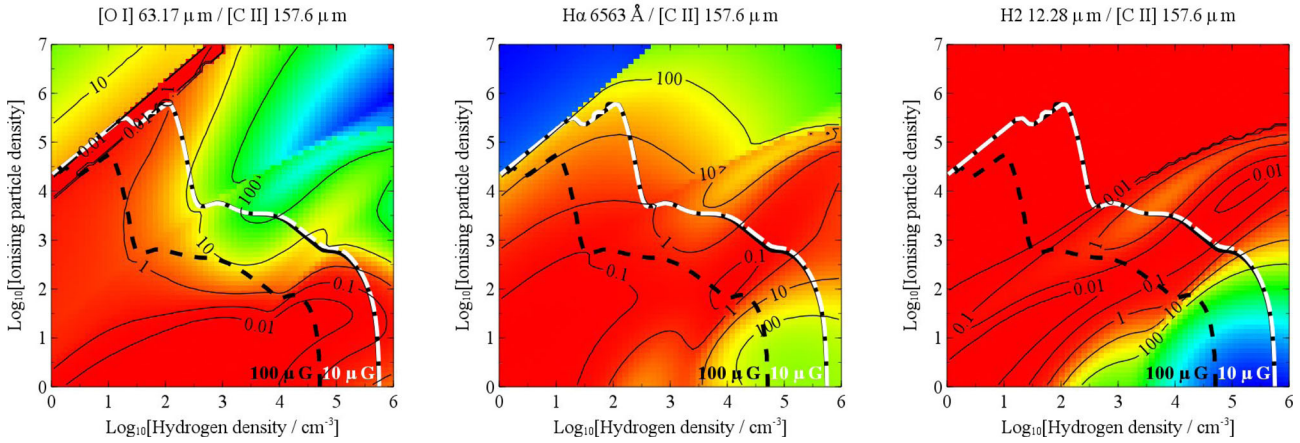

Figure 8. The ratios of key lines overlaid with contours of gas pressure in the cases where none, 10 μG and 100 μG fields are present in the gas. As in Fig. 7 the grids were recalculated with differing magnetic field strengths but the variations in the shown line ratios are negligible so we plot them here on one grid. Left: [O I] λ63 μm/[C II] λ157 μm . Middle: Hα/[C II] λ157 μm . Right: H_2 12.28 μm/[C II] λ157 μm . The measured fluxes are the integral of the cloudlets, indicated by the pressure contour. Observationally, the fluxes are [O I] λ63 μm/[C II] λ157 μm $\lesssim 1$, Hα/[C II] λ157 μm ∼1.3 (Mittal et al. 2012; Werner et al. 2014) and H_2 12 μm/[C II] λ157 μm ∼0.025 (F2009).

3.5 Words of caution

The models presented above explore the effect of the relaxation of certain assumptions, namely, the assumption of a power law in density, optically thin gas and no turbulent or magnetic pressure support to the gas. However, we relax these assumptions one by one. In nature, we may expect more than one of these effects to be present in the gas which will clearly introduce degeneracies but in the interests of presenting simple testable models we do not explore the entire parameter space. It is therefore important to consider this when devising observational strategies to test the model. We discuss the models and observations which may be robust tests of these models in the next section.

4 PREDICTIONS AND DISCUSSION

Extended cool/cold gaseous filaments are observed in BCGs yet, in most cases, apparently have very low star formation efficiencies. The question of what may be preventing the gas from cooling – what is its excitation/heating mechanism – is an important one as it goes to the heart of how much can cooling hot X-ray gas affect late stage galaxy evolution. In this paper we hope to provide testable predictions for the 'particle' excitation mechanism and to elucidate the importance of the surrounding hot gas in inhibiting the coldest/densest gas from forming and hence preventing star formation.

Making the assumption that the model put forward in F2009 and explored further here is the dominant excitation mechanism of the ionized and cold gas phases we can make predictions for further high spatial resolution cold gas observations of these filaments. The high spatial resolution of ALMA and *HST* is important as deriving gas masses and measuring the turbulent velocity of the filaments are highly dependent on the assumed gas fraction within the beam and on whether we are observing one or many filament threads. In Section 3 we look at the effects, on the [O I] λ63 μm and [C II] λ157 μm line ratios in the model, of relaxing one by one some of the assumptions of F2009. Many mechanisms may be playing a

part in setting the line ratios. However, applying Occam's razor we wish to single out a possible dominant mechanism.

Observations have found that the ratios of [C II] λ157 μm /Hα are approximately 0.8, [O I] λ63 μm/[C II] λ157 μm <1 and where it has been possible to measure the typically weak [O I] λ145 μm emission line the ratio of [O I] λ63 μm/[O I] λ145 μm ∼5–30 (Mittal et al. 2011, 2012; Werner et al. 2013, 2014). As discussed in Sections 3.1, the addition of a sink of very cold clouds at temperatures ∼10 K cannot explain the FIR line ratios while maintaining the ratios observed in the optical and NIR if the gas is all at constant pressure with the surrounding X-ray gas. [C II] λ157 μm becomes optically thick at a greater column than [O I] λ63 μm (see Appendix B) and the high [O I] λ63 μm/[O I] λ145 μm line ratios also rule out these emission lines being optically thick and suggest they come from the warm 50–100 K gas (see Fig. 6). Masing and foreground absorption in the [O I] lines can change these ratios but would tend to lower rather than increase the ratio (see discussion in Liseau et al. 2006).

Assuming the clouds maintain constant pressure with the hot ICM the most promising scenario would be to include an additional, density-dependent, pressure term. Increasing the pressure support in this density-dependent fashion, such as through an increase in the turbulence or density-dependent magnetic fields pushes the ratio of both [O I] λ63 μm/Hα and [C II] λ157 μm /Hα to lower ratios for a range of pressures and power-law indexes. An additional pressure support such as this would leave the pressure contribution from the hot gas essentially the same while requiring less thermal pressure from the dense gas, changing the line ratios that are predicted from cold, dense clouds while not altering the line ratios from the 10 000 K, 'warm', gas. If turbulence contributes all the additional pressure support then 2–10 $\mathrm{km\,s^{-1}}$ turbulence is required to reach the observed line ratios of approximately unity. This additional support decreases the density of the cold gas and could therefore also explain the longevity of the filaments.

Other indications exist that thermal pressure support alone is unlikely to be able to keep the filaments in BCGs stable for long periods of time. The periodicity observed in the star formation regions of the filaments of NGC 1275 would require turbulence of ∼17 $\mathrm{km\,s^{-1}}$ if all the additional pressure support came from turbulence (Canning et al. 2014). However, we note that the linear structure and long lifetimes suggest some pressure support likely comes from magnetic fields. Additionally, in radio-galaxies, quiescent, out-flowing cold clouds are often observed (e.g. Nesvadba et al. 2010; Combes et al. 2013; Alatalo et al. 2014), albeit at greater velocities than filaments from typical 'mechanical AGN feedback' in BCGs. Guillard et al. (2015) show that turbulent energy seeded by the AGN feedback could be responsible for the bright [C II] λ157 μm emission lines observed in these sources.

Whilst the FIR lines observed by Herschel offer important diagnostics of the gas properties, estimating the total mass in the very cold gas still requires an extrapolation of the model to the coldest emission lines $\lesssim$20 K. Most current observations of CO have observed the low J levels which are likely to be optically thick and therefore unable to constrain the gas masses. Future observations targeting optically thin CO lines will help answer the question of how much mass is concealed in the cold gas in massive galaxies and therefore the efficiencies of their star formation rates.

4.1 Model predictions

The model we are advocating in this paper is one where the excitation is dominated by collisions with energetic particles creating pockets of partially ionized regions interspersed with molecular regions in the filaments in a 'Swiss-cheese-like' fashion. The gas is supported also by magnetic fields or modest turbulence, which itself could be seeded by the impinging particles, which add pressure support to the gas, lowing the density and preventing immediate collapse into stars. In this section we outline tests of this model and diagnostics of the conditions of the gas.

4.1.1 [O I] λ63 μm/[O I] λ145 μm and [O I] λ63 μm/[C II] λ157 μm

Our models show, for optically thin emission, in low-temperature gas $\lesssim$150 K the [O I] λ63 μm/[C II] λ157 μm ratio traces relatively well the pressure. So, for fixed temperature the ratio can be used as a density diagnostic. In the left-hand panel of Fig. 9 we provide a plot of the optically thin line ratios of [O I] λ63 μm/[C II] λ157 μm against density for gas with temperatures ranging between 15 and 100 K. The current values of the ratio from Herschel observations are indicated by the grey region. Taking the gas to be ∼60 K, consistent with the [O I] λ63 μm/[O I] λ145 μm in the optically thin limit, in the right hand panel we plot the [O I] λ63 μm/[O I] λ145 μm against the [O I] λ63 μm/[C II] λ157 μm ratios and indicate the densities. Current observations, where at least two of these lines are detected, are overplotted. For gas under these conditions the current observations indicate the density should be a few 10^3 $\mathrm{cm^{-3}}$. It is important to note that these ratios are for the total galaxy fluxes which include the denser and in some cases star-forming interiors as well as the extended filaments.

4.1.2 High J CO emission lines and high-density gas tracers

Observations of the high J (J = 3–2 or higher) CO rotation ladder with ALMA will shed further light on the excitation mechanism and the importance of both turbulence and magnetic fields. Observing high J transitions is important for three key reasons. First, the high J transitions are insensitive to the low-temperature integration limits (see Fig. 1); secondly, they are less likely to be optically thick than the low J CO lines; and thirdly, the shape of the high J rotation ladder will enable a sensitive determination of the gas temperature; we might expect the gas temperature to differ from the dust temperature if the gas is excited by energetic particles as is seen in the molecular clouds in the nuclear disc of the Galaxy (e.g. Yusef-Zadeh, Wardle & Roy 2007).

The ratios of these high J CO lines to Hα are also a sensitive test of the presence of gas with densities greater than 10^3 (see Fig. 3), which allows limits to be placed on the levels of additional pressure support allowed as the assumption of total pressure equilibrium therefore enforces constant density cooling at very low temperatures. High-density lines like those of HCN and $\mathrm{HCO^+}$ ($n \gtrsim 10^4$ $\mathrm{cm^{-3}}$) should not be observed in the extended non-star-forming filaments if the additional pressure support is equivalent to 10 $\mathrm{km\,s^{-1}}$ turbulence. Salomé et al. (2008b) have detected HCN (3–2) in the central regions of NGC 1275 but so far no detection of very dense gas in the extended regions of filaments has been observed. Fig. C2 shows the expected emissivities of CO J(3–2), CO J(5–4), HCN and $\mathrm{HCO^+}$ for a range of ionizing particle fluxes and gas densities; the emissivity in these lines is highly density dependent. Constraining the density of the gas allows us to identify the level of additional pressure support and whether the clouds remain in pressure equilibrium in the coldest $\lesssim$20 K gas. Additionally, high

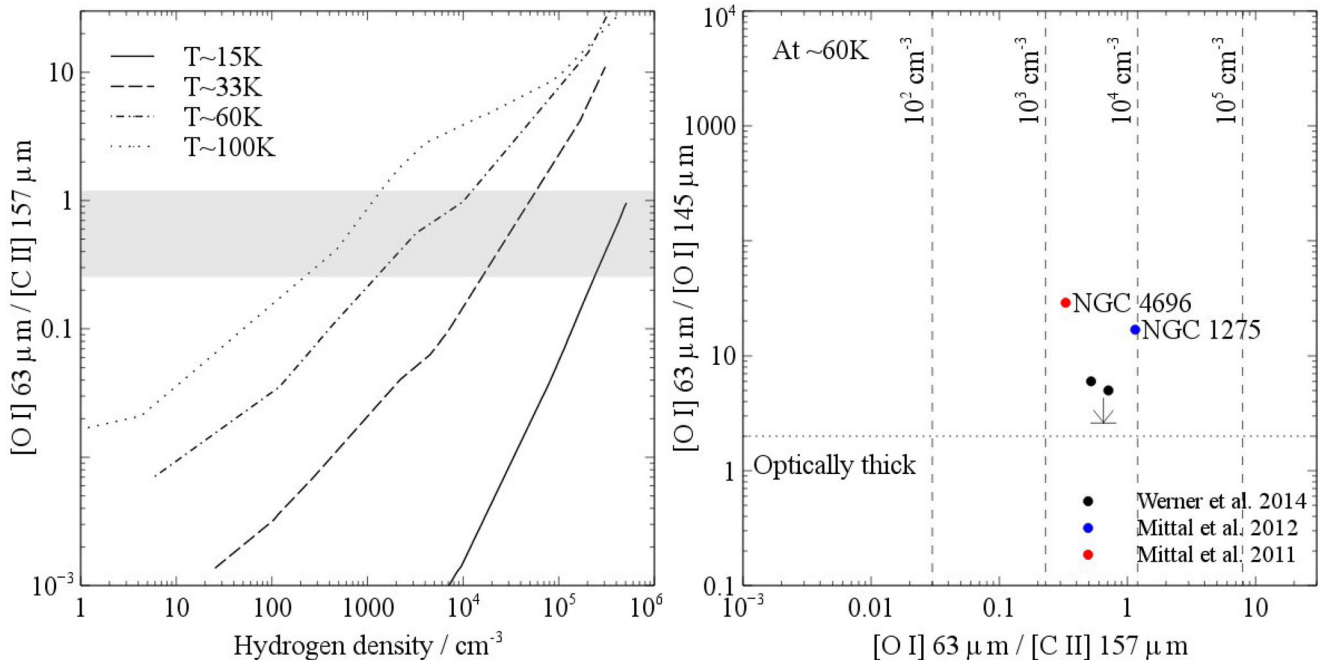

Figure 9. Left: if the gas is optically thin then at reasonable temperatures and densities the [O I] λ63 μm/[C II] λ157 μm ratio traces fairly well the gas pressure. Therefore, at constant temperature (or density) we can use the ratio as a density (or temperature) diagnostic. Here, we plot the emission lines ratio against the density for clouds of different temperatures. The grey band indicates the detected line ratios in some BCGs and gE galaxies. Right: a [O I] λ63 μm/[O I] λ145 μm versus [O I] λ63 μm/[C II] λ157 μm diagnostic diagram for a cloud at 60 K.

spatial resolution spectroscopy with ALMA will enable us to measure the turbulent support in the cold gas. Putting these together we can also elucidate the level of magnetic support required to the total pressure budget.

4.1.3 Low J ^{12}CO emission lines

Optical depth estimates from the ^{12}CO *J*(1–0) emission lines suggest this line is optically thick in the filaments of BCGs (Salomé & Combes 2003; Salomé et al. 2011; note that ^{13}CO and C^{18}O are likely to be optically thin in the filaments and as such may be good diagnostics of the model). Ratios of these lines with other detected emission lines are thus not easily compared to predictions from our model. However, these lines are likely thermalized and can be used as sensitive thermometers for the gas as the excitation temperature will be equal to the kinetic temperature. Combined with ratios of high *J* emission lines of CO which are sensitive tracers of the density (see Fig. C2) constraints can be put on the physical conditions of the coldest gas.

We have argued above that collisional excitation with the hot particles in the surrounding X-ray gas may inhibit the dense conditions required for star formation in the extended filaments. However, we know of a few cases in which some filaments have disrupted into stars (e.g. McDonald & Veilleux 2009; O'Dea et al. 2010; Canning et al. 2014). In regions in which young stars are observed obviously emission lines dominated by excitation from young stellar sources will be observed. We might also expect the turbulence to be higher in these regions due to driving from young stellar winds hence the diagnostics suggested above are not relevant to regions which are actively forming stars and should not be applied to star-forming knots in filaments.

However, some information may still be gleamed from studying these regions. Additional pressure support of the gas, either by turbulence or by magnetic fields, should alter the Jeans mass. Collisional excitation with energetic particles from the surrounding gas heats the gas and increases its ionization fraction which will increase its coupling to magnetic fields, which should slow the time-scale for gravitational collapse. We speculate that this excitation mechanism could therefore lead to a top heavy IMF in the filaments, explaining the very massive star clusters observed in some outer filaments (Canning et al. 2014).

4.2 The source of ionizing particles

The model described above requires ionization rates of up to 10^6 times the Galactic cosmic ray background density. F2009 conclude that these ionizing particles are unlikely to come from a population of relativistic particles similar to our Galactic cosmic ray population. Potentially, the suprathermal electrons could originate from magnetic reconnection within the filaments (Churazov et al. 2013), the surrounding hot intra-group and ICM (Fabian et al. 2011) or from photoionization by a source with a very hard ionizing spectrum. Little is known of the strength or structural properties of the magnetic fields which may penetrate these filaments; however, if the soft X-ray flux from regions where the optical filaments exist signposts the interaction of these multiphase filaments and the hot gas then the particle flux expected to penetrate the filaments is of the order of 10^6 particles s^{-1} cm^{-2} (Fabian et al. 2011), roughly the required rate for our spectral models. An additional hard photoionizing source, such as very young, massive stars or AGN, is unlikely for two reasons; first, the line ratios in the filaments are remarkably similar over large distances (e.g. Lim et al. 2012) and, secondly, if

the ionization is from bright, massive stars these should be seen in the filaments.

5 CONCLUSIONS

We have extended the particle heating mechanism first presented in F2009 to examine the effects of abundant cold clouds, optically thick gas, turbulence and magnetic fields on the bright line ratios from cold, $\lesssim$100 K, gas. We explore these models in the context of extended cool and cold gaseous nebulae observed in some massive galaxies many of which are devoid of star formation. We wish to be clear that we are not considering the centrally peaked emission and associated star-forming regions observed in many massive galaxies where it is clear that many processes are occurring. We focus instead on 'clean' non-star-forming, extended nebulae.

We suggest the simplest explanation for the discrepancy between the predicted [C II] and [O I] line ratios may be that there is a small amount of additional pressure support in the cold gas from either turbulence (2–10 km s^{-1}) and/or density-dependent magnetic fields, and we present predictions for line ratios and diagnostics of the gas temperatures and densities. We suggest that turbulence may be driven by the influx of energetic particles impinging on the cold gas, creating a higher level of ionization in the gas and decreasing the gas density which could also inhibit star formation in these filaments. The majority of filaments would remain long lived unless the gas pressure drops, star formation is either triggered by external perturbations, such as disturbances from rising AGN bubbles or galaxy interactions or the heat from such external perturbations is strong enough to eradicate the filaments.

ACKNOWLEDGEMENTS

We thank the referee for helpful comments which greatly improved the paper. This work is based in part on observations made with Herschel, a European Space Agency Cornerstone Mission with significant participation by NASA. Support for this work was provided by NASA through award number 1428053 issued by JPL/Caltech. GJF acknowledges support by NSF (1108928, 1109061, and 1412155), NASA (10-ATP10-0053, 10-ADAP10-0073, NNX12AH73G, and ATP13-0153), and STScI (HST-AR-13245, GO-12560, HST-GO-12309, GO-13310.002-A, and HST-AR-13914). ACF thanks the ERC for Advanced Grant Feedback. REAC thanks E. Churazov, B. Mathews and J. Pringle for helpful and interesting discussions and for reading a version of the manuscript. The contour plots were produced with the VEUSZ plotting program (http://home.gna.org/veusz/).

REFERENCES

Alatalo K. et al., 2014, ApJ, 795, 159
Allen S. W., 1995, MNRAS, 276, 947
Bakes E. L. O., Tielens A. G. G. M., 1994, ApJ, 427, 822
Canning R. E. A., Fabian A. C., Johnstone R. M., Sanders J. S., Conselice C. J., Crawford C. S., Gallagher J. S., Zweibel E., 2010, MNRAS, 405, 115
Canning R. E. A., Fabian A. C., Johnstone R. M., Sanders J. S., Crawford C. S., Ferland G. J., Hatch N. A., 2011, MNRAS, 1443
Canning R. E. A. et al., 2013, MNRAS, 435, 1108
Canning R. E. A. et al., 2014, MNRAS, 444, 336
Cavagnolo K. W., Donahue M., Voit G. M., Sun M., 2008, ApJ, 683, L107
Cazaux S., Tielens A. G. G. M., 2002, ApJ, 575, L29
Chatzikos M. et al., 2015, MNRAS, 446, 1234
Churazov E., Ruszkowski M., Schekochihin A., 2013, MNRAS, 436, 526
Combes F. et al., 2013, A&A, 558, A124
Conselice C. J., Gallagher J. S., III, Wyse R. F. G., 2001, AJ, 122, 2281
Crawford C. S., Allen S. W., Ebeling H., Edge A. C., Fabian A. C., 1999, MNRAS, 306, 857
Crawford C. S., Hatch N. A., Fabian A. C., Sanders J. S., 2005, MNRAS, 363, 216
Donahue M., Mack J., Voit G. M., Sparks W., Elston R., Maloney P. R., 2000, ApJ, 545, 670
Donahue M. et al., 2010, ApJ, 715, 881
Donahue M., de Messières G. E., O'Connell R. W., Voit G. M., Hoffer A., McNamara B. R., Nulsen P. E. J., 2011, ApJ, 732, 40
Edge A. C., 2001, MNRAS, 328, 762
Edge A. C., Wilman R. J., Johnstone R. M., Crawford C. S., Fabian A. C., Allen S. W., 2002, MNRAS, 337, 49
Edge A. C. et al., 2010a, A&A, 518, L47
Edge A. C. et al., 2010b, A&A, 518, L46
Fabian A. C., 2012, ARA&A, 50, 455
Fabian A. C., Johnstone R. M., Sanders J. S., Conselice C. J., Crawford C. S., Gallagher J. S., III, Zweibel E., 2008, Nature, 454, 968
Fabian A. C., Sanders J. S., Williams R. J. R., Lazarian A., Ferland G. J., Johnstone R. M., 2011, MNRAS, 417, 172
Falcke H., Rieke M. J., Rieke G. H., Simpson C., Wilson A. S., 1998, ApJ, 494, L155
Farage C. L., McGregor P. J., Dopita M. A., 2012, ApJ, 747, 28
Ferland G. J., Fabian A. C., Hatch N. A., Johnstone R. M., Porter R. L., van Hoof P. A. M., Williams R. J. R., 2008, MNRAS, 386, L72
Ferland G. J., Fabian A. C., Hatch N. A., Johnstone R. M., Porter R. L., van Hoof P. A. M., Williams R. J. R., 2009, MNRAS, 392, 1475 (F2009)
Ferland G. J. et al., 2013, Rev. Mex. Astron. Astrofis., 49, 137
Field G. B., 1965, ApJ, 142, 531
Glassgold A. E., Langer W. D., 1973, ApJ, 186, 859
Guillard P., Boulanger F., Lehnert M. D., Pineau des Forêts G., Combes F., Falgarone E., Bernard-Salas J., 2015, A&A, 574, A32
Hatch N. A., Crawford C. S., Fabian A. C., Johnstone R. M., 2005, MNRAS, 358, 765
Heckman T. M., Baum S. A., van Breugel W. J. M., McCarthy P., 1989, ApJ, 338, 48
Heiles C., Crutcher R., 2005, in Wielebinski R., Beck R., eds, Lecture Notes in Physics, Vol. 664, Cosmic Magnetic Fields. Springer Verlag, Berlin, p. 137
Hennebelle P., Chabrier G., 2013, ApJ, 770, 150
Hicks A. K., Mushotzky R., 2005, ApJ, 635, L9
Hicks A. K., Mushotzky R., Donahue M., 2010, ApJ, 719, 1844
Hollenbach D. J., Tielens A. G. G. M., 1997, ARA&A, 35, 179
Hollenbach D. J., Tielens A. G. G. M., 1999, Rev. Modern Phys., 71, 173
Hubble E., Humason M. L., 1931, ApJ, 74, 43
Indriolo N., Geballe T. R., Oka T., McCall B. J., 2007, ApJ, 671, 1736
Jaffe W., Bremer M. N., 1997, MNRAS, 284, L1
Jaffe W., Bremer M. N., van der Werf P. P., 2001, MNRAS, 324, 443
Jaffe W., Bremer M. N., Baker K., 2005, MNRAS, 360, 748
Johnstone R. M., Fabian A. C., 1988, MNRAS, 233, 581
Johnstone R. M., Fabian A. C., Nulsen P. E. J., 1987, MNRAS, 224, 75
Johnstone R. M., Hatch N. A., Ferland G. J., Fabian A. C., Crawford C. S., Wilman R. J., 2007, MNRAS, 382, 1246
Johnstone R. M., Canning R. E. A., Fabian A. C., Ferland G. J., Lykins M., Porter R. L., van Hoof P. A. M., Williams R. J. R., 2012, MNRAS, 425, 1421
Kritsuk A. G., Norman M. L., 2011, preprint (arXiv:1111.2827)
Larson R. B., 1981, MNRAS, 194, 809
Lim J., Ohyama Y., Chi-Hung Y., Dinh-V-Trung, Shiang-Yu W., 2012, ApJ, 744, 112
Liseau R., Justtanont K., Tielens A. G. G. M., 2006, A&A, 446, 561
McDonald M., Veilleux S., 2009, ApJ, 703, L172
McDonald M. et al., 2012, Nature, 488, 349
McNamara B. R., O'Connell R. W., 1989, AJ, 98, 2018
McNamara B. R., Wise M. W., Murray S. S., 2004, ApJ, 601, 173
McNamara B. R. et al., 2006, ApJ, 648, 164
McNamara B. R. et al., 2014, ApJ, 785, 44

Maloney P. R., Hollenbach D. J., Tielens A. G. G. M., 1996, ApJ, 466, 561
Mittal R. et al., 2011, MNRAS, 418, 2386
Mittal R. et al., 2012, MNRAS, 426, 2957
Nesvadba N. P. H. et al., 2010, A&A, 521, A65
O'Dea C. P. et al., 2008, ApJ, 681, 1035
O'Dea K. P. et al., 2010, ApJ, 719, 1619
Oonk J. B. R., Jaffe W., Bremer M. N., van Weeren R. J., 2010, MNRAS, 405, 898
Predehl P., Schmitt J. H. M. M., 1995, A&A, 293, 889
Quillen A. C. et al., 2008, ApJS, 176, 39
Rafferty D. A., McNamara B. R., Nulsen P. E. J., 2008, ApJ, 687, 899
Richardson C. T., Baldwin J. A., Ferland G. J., Loh E. D., Kuehn C. A., Fabian A. C., Salomé P., 2013, MNRAS, 430, 1257
Russell H. R. et al., 2014, ApJ, 784, 78
Sabra B. M., Shields J. C., Filippenko A. V., 2000, ApJ, 545, 157
Salomé P., Combes F., 2003, A&A, 412, 657
Salomé P. et al., 2006, A&A, 454, 437
Salomé P., Revaz Y., Combes F., Pety J., Downes D., Edge A. C., Fabian A. C., 2008a, A&A, 483, 793
Salomé P., Combes F., Revaz Y., Edge A. C., Hatch N. A., Fabian A. C., Johnstone R. M., 2008b, A&A, 484, 317
Salomé P., Combes F., Revaz Y., Downes D., Edge A. C., Fabian A. C., 2011, A&A, 531, A85
Sanders J. S., Fabian A. C., 2007, MNRAS, 381, 1381
Shull J. M., van Steenberg M. E., 1985, ApJ, 298, 268
Sparks W. B., Macchetto F., Golombek D., 1989, ApJ, 345, 153
Sparks W. B. et al., 2012, ApJ, 750, L5
Sparks W. B. et al., 2014, ApJ, 780, 66
Tassis K., Christie D. A., Urban A., Pineda J. L., Mouschovias T. C., Yorke H. W., Martel H., 2010, MNRAS, 408, 1089
Taylor G. B., Gugliucci N. E., Fabian A. C., Sanders J. S., Gentile G., Allen S. W., 2006, MNRAS, 368, 1500
Terlevich R., Melnick J., 1985, MNRAS, 213, 841
van Hoof P. A. M., Weingartner J. C., Martin P. G., Volk K., Ferland G. J., 2001, in Ferland G., Savin D. W., eds, ASP Conf. Ser. Vol. 247, Spectroscopic Challenges of Photoionized Plasmas. Astron. Soc. Pac., San Francisco, p. 363
van Hoof P. A. M., Weingartner J. C., Martin P. G., Volk K., Ferland G. J., 2004, MNRAS, 350, 1330
Vazquez-Semadeni E., 1994, ApJ, 423, 681
Voit G. M., 1991, ApJ, 377, 158
Voit G. M., Donahue M., 1997, ApJ, 486, 242
Werner N. et al., 2013, ApJ, 767, 153
Werner N. et al., 2014, MNRAS, 439, 2291
Wilman R. J., Edge A. C., Johnstone R. M., Fabian A. C., Allen S. W., Crawford C. S., 2002, MNRAS, 337, 63
Wilman R. J., Edge A. C., Swinbank A. M., 2009, MNRAS, 395, 1355
Xu Y., McCray R., 1991, ApJ, 375, 190
Yusef-Zadeh F., Wardle M., Roy S., 2007, ApJ, 665, L123

APPENDIX A: CLOUDY CODE

```
c
c
table HM05 z = 0
extinguish by 21, leakage = 0
cmb redshift 0
c
c
atom H2 levels large
atom H-like Lyman pumping off
abundances he = -1.022 li = -10.268 be = -20.000 b = -10.051 c = -3.523 n = -4.155
continue o = -3.398 f = -20.000 ne = -4.222 na = -6.523 mg = -5.523 al = -6.699
continue si = -5.398 p = -6.796 s = -5.000 cl = -7.000 ar = -5.523 k = -7.959
continue ca = -7.699 sc = -20.000 ti = -9.237 v = -10.000 cr = -8.000 mn = -7.638
continue fe = -5.523 co = -20.000 ni = -7.000 cu = -8.824 zn = -7.6990 no grains
grains ism
grains pah
set pah constant -4.6
set H2 Jura rate
case B
c
c
cosmic rays background -1 vary
grid from 0 to 7 in 0.1 dex steps
hden 4 vary
grid 0 6 0.1
c
c
stop zone 1
set dr 0
stop temperature off
turbulence = 2 km/s
```

APPENDIX B: OPTICAL DEPTHS

In Fig. B1, we have shown the emission-line emissivity divided by the cloud column density against the cloud column density for two models. The first has a hydrogen density of $10^{5.3}$ cm^{-3} and a particle density of 10^2 times that of the Galactic background cosmic ray energy density (the Galactic background is here taken as 1.8 eV cm^{-3}), which results in a cloud surface temperature of $\sim$15 K. We choose this temperature and density model as an optically thin gas under these conditions has [O I] λ63 μm over [C II] λ157 μm less than one. The second has a hydrogen density of $10^{5.0}$ cm^{-3} and a particle density of $10^{2.5}$ times that of the Galactic background cosmic ray energy density leading to a higher temperature, $\sim$33 K. This is close to the temperature at which the emission expected from both lines is equal for an optically thin gas under these pressure conditions (both models have a pressure of $\sim 10^{6.5}$ cm^{-3} K; see Fig. 1).

For an optically thin line, the emissivity will increase in proportion to the column; this produces horizontal lines on the plots. The column density at which the column begins to increase faster than the emissivity indicates the column at which the line has become optically thick and line photons are collisionally deexcited following multiple scatterings. The [O I]63 μm line in the shown model (upper left plot) becomes optically thick around a column density of $\sim 10^{22}$ cm^{-2}, corresponding to a high extinction of $A_V = 5.6$, assuming $N_H = 1.8 \times 10^{21} A_V$ (Predehl & Schmitt 1995). The [O I] λ145 μm and [C II] λ157 μm emission lines become optically thick at columns greater than $\sim 10^{22.5}$ cm^{-2}, which are very rare and so these lines are likely optically thin.

In the right hand panels, we show the emissivities in the CO rotation ladder as a function of column density. The low J lines of CO have large optical depths in gas with low extinction $A_V < 1$ and are most likely optically thick. These lines may not be constraining to test the various excitation models of the filaments but can be sensitive thermometers of the gas temperature.

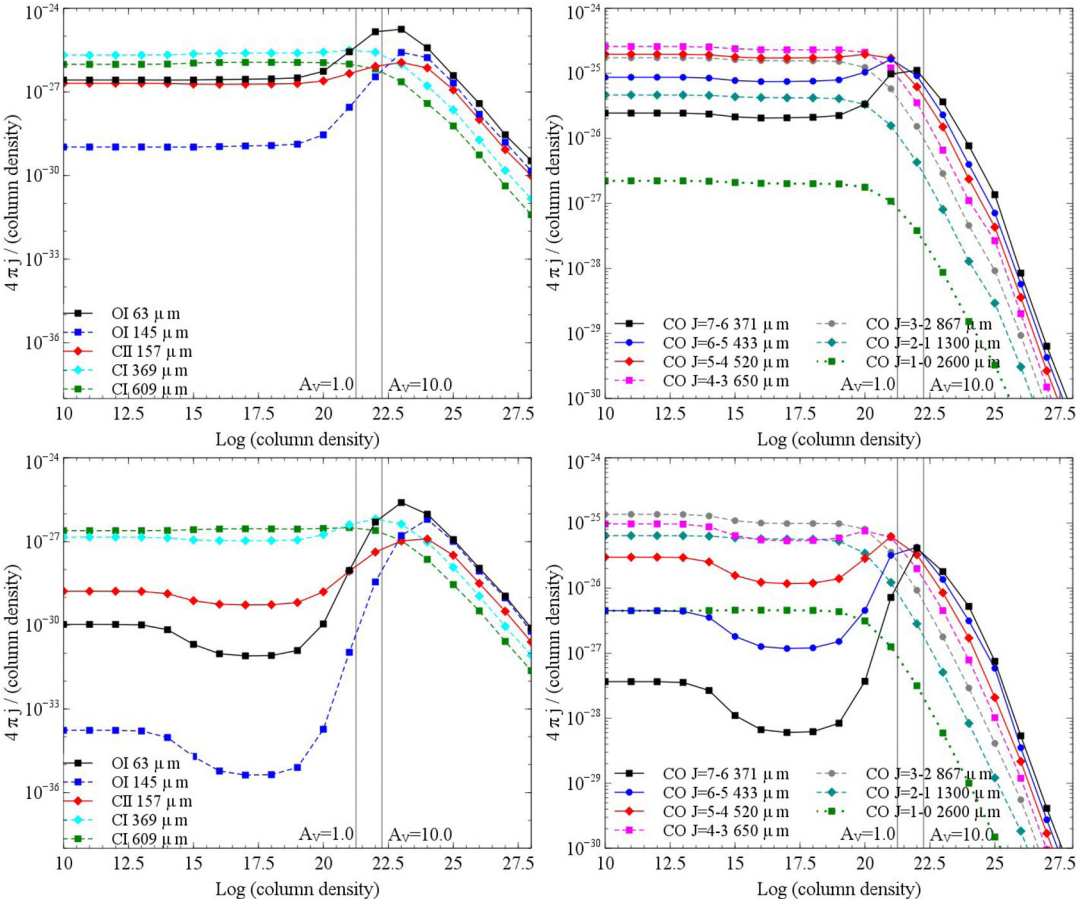

Figure B1. The predicted line emissivity divided by the column density plotted against the column density of the clouds for clouds at constant pressure. The surface temperature of the cloud in the upper plot is $T \sim 33$ K while the lower plot has a lower surface temperature of $T \sim 15$ K.

APPENDIX C: EMISSIVITIES

For completeness, in Figs C1 and C2 we show the optically thin emissivities of other key strong lines from our model and the ratios for the neutral carbon and oxygen lines. In the cold gas the optically thin [O I] line ratios are a relatively faithful indicator of the gas temperature while the [C I] ratios are more sensitive to the particle ionizing flux. The lines shown in Fig. C2 are good indicators of the gas density.

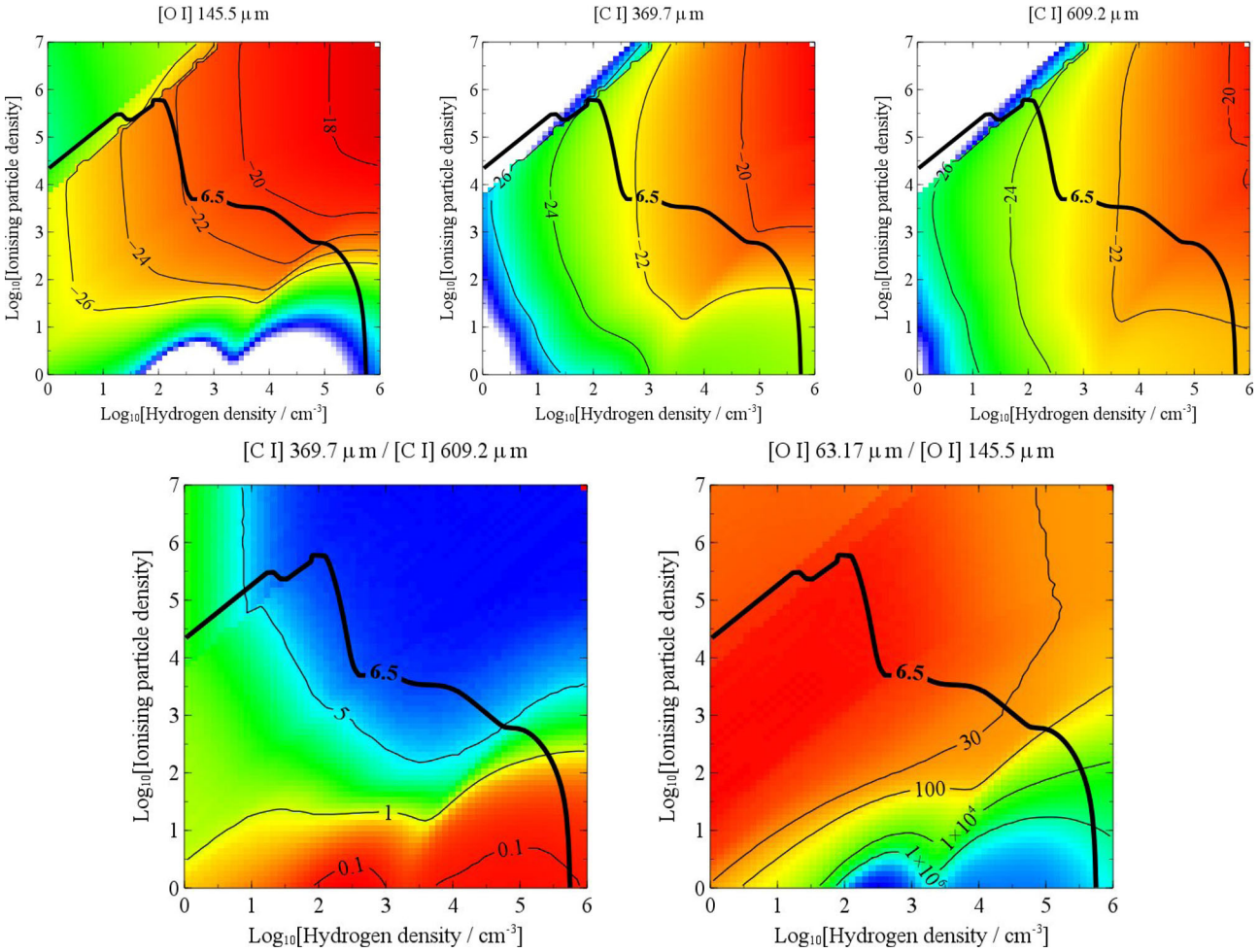

Figure C1. Predicted log emissivities of the [O I] λ145 μm, [C I] λ369 μm, and [C I] λ609 μm transitions and the neutral carbon and neutral oxygen line ratios for an optically thin gas. The contour indicates a gas pressure of $10^{6.5}$ cm^{-3} K.

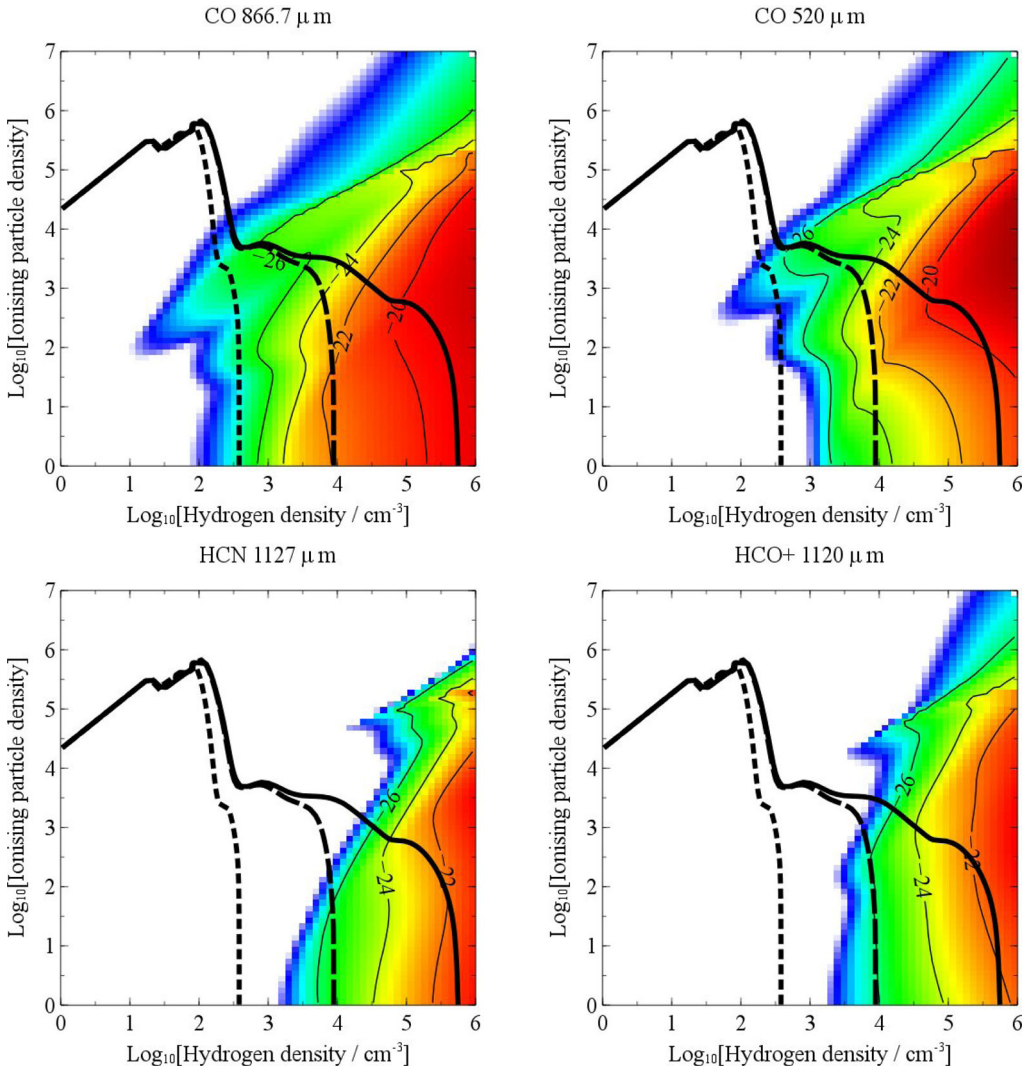

Figure C2. The predicted log emissivities of the CO J(3–2) and J(5–4) transitions and those of lines of HCN and HCO+ overlaid with contours of the gas pressure as shown in Fig. 7. All these lines offer sensitive diagnostics of the gas density and the CO ladder transitions can also offer sensitive temperature measurements. If a high degree of additional pressure support is present in the filaments than the densest gas should not be. Observations of the strength of these density sensitive lines in regions in which no star formation is occurring can constrain the additional pressure support in the gas.

This paper has been typeset from a TEX/LATEX file prepared by the author.